E13-2018-22

N. V. Korepanova *, N. D. Dikusar,
Yu. N. Pepelyshev, M. Dima [1]

NEUTRON NOISE ANALYSIS USING THE BASIC ELEMENT METHOD

Submitted to "Annals of Nuclear Energy"

* On leave at the Institute of Modern Physics, Chinese Academy of Science, Lanzhou, China
[1] Institute for Physics and Nuclear Engineering, DFCTI, Bucharest

Корепанова Н. В. и др. E13-2018-22

Анализ нейтронного шума с использованием метода базисных элементов

Полный диапазон шумов энергии импульсов при нормальных условиях работы реактора ИБР-2М (ОИЯИ, Дубна) достигает $\pm 22\,\%$. Поэтому медленно изменяющаяся средняя мощность вследствие, например, движения регулирующих органов «тонет» в шумах. Но в ряде случаев именно эти медленные компоненты изменения энергии импульсов — так называемые базисные сигналы (базовая линия) — имеют принципиальное значение для обоснования условий безопасной работы реактора. Для определения базовой линии в шумах ИБР-2М используется среднеквадратичная кусочно-полиномиальная аппроксимация шестого порядка (СКПА-6). Алгоритм СКПА-6 зависит от параметров управления α, β, M и K, оптимальные значения которых зависят от исходных параметров шумов. Алгоритм примененяется как к статическому, так и динамическому состоянию реактора в диапазоне средней мощности 30 кВт – 2 МВт. Среднее время обработки одной точки на ПК x86_64 Processor Intel Core i5-4570 Sandy Bridge machine, 3,20 ГГц, составляет 0,05 мс, что позволяет использовать алгоритм СКПА-6 в режиме реального времени.

Работа выполнена в Лаборатории нейтронной физики им. И. М. Франка и Лаборатории информационных технологий ОИЯИ.

Препринт Объединенного института ядерных исследований. Дубна, 2018

Korepanova N. V. et al. E13-2018-22

Neutron Noise Analysis Using the Basic Element Method

The full range of noise energy pulses reaches $\pm 22\%$ under normal conditions of operation of the IBR-2M reactor (JINR, Dubna). Therefore, slow changes in average power, caused, for example, by the movement of regulatory bodies, “drown” in the noises. But in a number of cases, it is these slow components of the pulse energy variation, the so-called basic signals (baseline), that are of fundamental importance for justifying the conditions for safe operation of the reactor. To determine the baseline in the noises of the IBR-2M the sixth order mean-square piecewise polynomial approximation (MSPPA-6) was used for the detection of the baseline in the noises of IBR-2M. The algorithm MSPPA-6 depends on control parameters α, β, M and K, the optimal values of which depend on the initial noise parameters. The algorithm was applied to both the static and the dynamic state of the reactor in the range of an average power of 30 kW – 2 MW. The average processing time of one point on a PC x86_64 Processor Intel Core i5-4570 Sandy Bridge machine, 3.20 GHz, was 0.05 ms, which allows using the MSPPA-6 algorithm in real time.

The investigation has been performed at the Frank Laboratory of Neutron Physics and the Laboratory of Information Technologies, JINR.

Preprint of the Joint Institute for Nuclear Research. Dubna, 2018

1. INTRODUCTION

Usually noise is an unwanted phenomenon. Most methods regarding noise are designed to suppress this factor; however, in some systems, such as nuclear reactor, noise, as fluctuation of the neutron flux [1], contains important information. Both the random nature of neutron processes and the work of external systems of a reactor (such as the coolant system, the safety system, etc.) are causes of neutron noise. On this basis the neutron noise can be used for estimating internal reactor parameters, such as reactivity, cross sections and time constants [1], and for diagnostic purposes. In the articles [2–4] an influence of reactor parameters on neutron noise and the estimation of some kinetic parameters for the IBR-2M reactor are presented. In all cases the extraction of noise from a recorded signal becomes a primary task.

In the case of IBR-2M (JINR, Dubna, Russia), neutron noise is represented by instantaneous changes of the pulse energy relative to its baseline. Casual changes of the energy of impulses in IBR-2M amount to $\pm 22\,\%$ of the average value. The baseline of the pulse energy varies itself also during reactor operation, mostly due to control rods, change in cooling agent flow rate (liquid sodium) and its temperature at core inlet, etc. Extracting neutron noise entails them a preprocessing part of finding baseline. Due to high computational demand, in order to allow real-time processing of high precision, a variant of the Basic Element Method [5–8] was adapted to solve this task.

2. THE IBR-2M REACTOR

The IBR-2M pulsed reactor of periodic operation (upgraded version of the IBR-2 reactor) was commissioned with an average power of 2 MW at the Frank Laboratory of Neutron Physics in 2012. The reactor generates short neutron pulses (200 μs at half-width) with a period of 0.2 s and an amplitude of 1830 MW. In the IBR-2M reactivity pulses are produced by the two reactivity modulators rotating near the core. The main (MMR) and auxiliary (AMR) movable reflectors are coaxially positioned and kinetically connected to one another. The MMR rotates at a rate of 600 rpm, and the AMR rotates at a rate of 300 rpm. As the movable reflectors rotate, they generate periodical reactivity pulses. When the

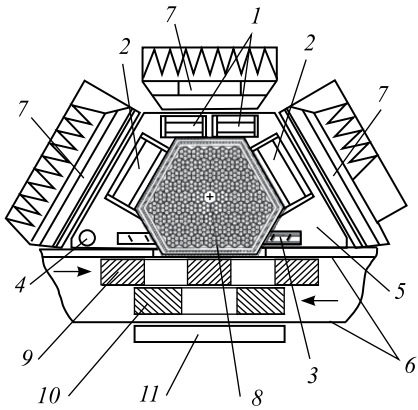

Fig. 1. Section of the IBR-2M active core: (*1*) emergency protection blocks, (*2*) compensation block, (*3*) intermediate control block, (*4*) automatic regulator, (*5*) stationary reflector, (*6*) movable reflector case, (*7*) grooved water moderators, (*8*) external neutron source, (*9*) main movable reflector (MMR), (*10*) auxiliary movable reflector (AMR), (*11*) flat water moderator

two reflectors pass the core simultaneously, a reactivity pulse develops and for a short time (450 μs) the reactor stops being in a super-critical state with prompt neutrons. As the reflectors move away from the reactor core, the reactor becomes deeply sub-critical. Such a reactivity modulation results in the neutron flux density increasing up to 10^{17} cm$^{-2} \cdot$ s^{-1}. The IBR-2M pulse shape is close to a truncated Gaussian distribution with a half-width at half-maximum of (200 ± 4) μs (see Fig. 2).

The reactor core is shaped as an irregular hexahedral prism positioned vertically. Two rotating movable reflectors pass beside one of the prism faces. Stationary reflectors, used for emergency protection (EP) and control of the reactor, adjoin five other faces. The schematic representation of a cross section of the IBR-2M is shown in Fig. 1. The active core comprises 69 fuel assemblies

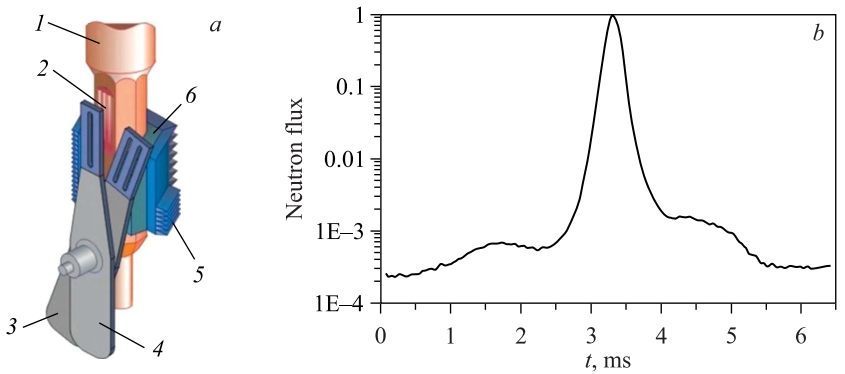

Fig. 2. *a*) IBR-2M: (*1*) reactor vessel, (*2*) active core, (*3*) main movable reflector (MMR), (*4*) auxiliary movable reflector (AMR), (*5*) grooved water moderators, (*6*) stationary reflector. *b*) Power pulse shape of the IBR-2M reactor

with plutonium dioxide as the reactor fuel. The active length of fuel assemblies is 444 mm. The reactor coolant is liquid sodium with a circulation activated by electromagnetic pumps.

There are four water moderators which serve to thermalize fast neutrons down to a thermal energy level. The IBR-2M serves 14 channels used for research in different fields of science, such as the physics of nano-systems, the dynamics of materials and investigation of their structure, molecular biology and pharmacology, investigation of the structure of rock and minerals, engineering diagnostics, etc. All the experimental equipment is based on the time-of-flight method.

3. DATA ACQUISITION

The source data are represented as an array of consecutive pulse energy values registered during reactor operation. The acquisition frequency corresponded to a succession of power pulse frequencies, which is equal to 5 Hz. The magnitude registered is proportional to the charge emitted in fission ionization chambers during the action of a power pulse. To exclude errors due to the detector shielding in the process of motion of the regulating elements in the power measurement process, data have been averaged from the measured indications of three independent detectors located around the core (see Fig. 3).

The gauge to the absolute power was carried out according to the heat release calibration measurements in the core. Data acquisition was realized by means of the reactor parameter measurement system. The time interval for approximation was chosen from the criterion of containing the dynamic reactor state (here, a rise of power) and the stationary reactor state at a power of 2 MW.

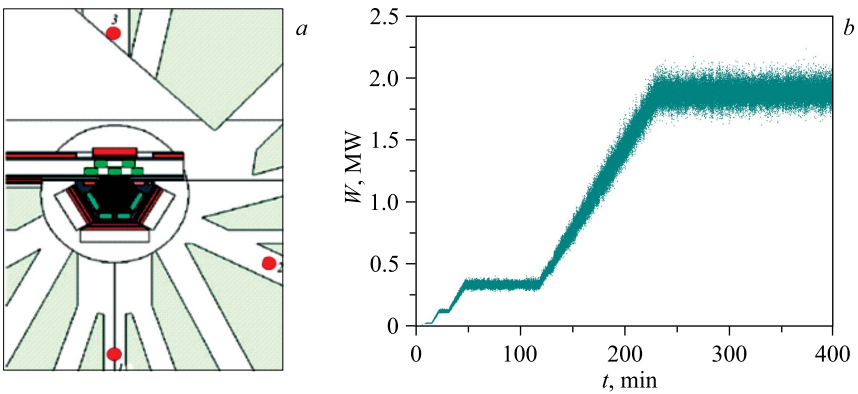

Fig. 3. Location of the fission ionization chambers: (*1*) 5th beam, 115 cm from the core center, (*2*) 8th beam, 119 cm from the core center, (*3*) 13th beam, 116 cm from the core center

4. THE BASIC ELEMENT METHOD (BEM)

The essence of the BEM is the representation of the polynomial $P_n(x) = \sum_{i=0}^{n} a_i\, x^i$ in a form of decomposition by four basic elements: w_1, w_2, w_3 (quadratic parabolas) and Q (a cubic parabola) [5]. The basic elements depend on the control parameters x_0, $\alpha = x_\alpha - x_0$ and $\beta = x_\beta - x_0$, where x_α, x_0, x_β are the beginning, middle and end of the interval, respectively (*the three point grid*). These parameters *relate* to the independent variable $\tau = x - x_0$, where x is the current position, by *a special cross-ratio rule* $[\xi_1\xi_2\xi_3\xi_4] = [13]/[23] : [34]/[14]$, $[ij] = \xi_j - \xi_i$, $\xi_j \neq \xi_i$.

For the quadruple $[\tau\alpha\beta 0]$ with a fixed first point τ, this rule generates three *fractional-rational* functions w_1, w_2, w_3 with respect to the parameters α, β and τ (*quadratic* functions relative to τ):

$$w_1 = \frac{-\tau(\tau-\beta)}{\alpha\gamma}, \quad w_2 = \frac{-\tau(\tau-\alpha)}{\beta\gamma},$$

$$w_3 = \frac{(\tau-\alpha)(\tau-\beta)}{\alpha\beta}, \quad \sum_{i=1}^{3} w_i = 1, \quad \gamma = \beta - \alpha.$$

The fourth element Q is *a zeroing* cubic parabola [7]:

$$Q = \alpha\beta\tau w_3 = \tau(\tau-\alpha)(\tau-\beta), \quad \alpha\beta\gamma \neq 0, \quad \alpha\beta < 0, \tau, \alpha, \quad \beta \in R.$$

The BEM-polynomial is built on the three-point grid $\Delta_3^{\alpha\beta} : \alpha < 0 < \beta$ by the transformation of the polynomial $P_n(x;\mathbf{c}) = \sum_{j=0}^{n} c_i (x - x_0)^i$ into a new form [5, 7, 8]:

$$P_{n\downarrow m} = \sum_{j=0}^{m} Q^j \mathbf{w}^T \mathbf{r}_j$$

or in the form of basis functions, as components of vectors $\mathbf{b}_j = [b_{1j},\, b_{2j},\, b_{3j}]^T$:

$$P_{n\downarrow m} = \sum_{j=0}^{m} \mathbf{b}_j^T \mathbf{r}_j = \sum_{j=0}^{m} \sum_{i=1}^{3} Q^j w_i r_{ij}, \quad \mathbf{b}_0 = \mathbf{w}, \quad m = \lfloor n/3 \rfloor .$$

The basis functions $b_{ij} = Q^j w_i$, $i = \overline{0,3}$, $j = \overline{0,m}$ are the polynomials of degree $3j+2$ with respect to τ and they have zeros at the nodes of the grid $\Delta_3^{\alpha\beta}$ (Fig. 4, *a*). The coefficients $\mathbf{r}_j = [r_{\alpha j},\, r_{\beta j},\, r_{0j}]^T$ depend on α, β and $P_n^{(j)}(x_\nu;\mathbf{c})$, $j = \overline{0,m}$, $\nu = \alpha, \beta, 0$. In Fig. 4, *b*, a geometrical interpretation for the BEM model of the 5th degree polynomial is given ($m = 1$).

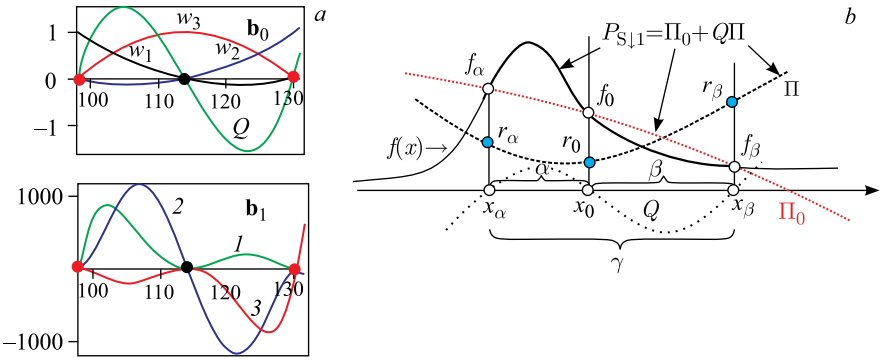

Fig. 4. The basis functions (a) and geometrical interpretation of BEM-polynomial $P_{5\downarrow1}(x,\alpha,\beta)$ (b)

We use a *mean-squares piecewise polynomial approximation* of the sixth order (MSPPA-6) to smooth the data from the IBR-2M on given interval $[a,b]$ (a global grid). When using BEM-polynomials for data smoothing, the solution is *optimized* (I) by using control parameters that affect the stability and accuracy of calculations, and (II) by *reducing the order of the derivatives* in comparison with the degree of the approximating polynomial in the calculation of $r_{\nu j}$, where $\nu=\alpha,\beta,0$ and $j=\overline{1,m}$ [6]. Increasing the degree of the polynomial reduces the number of nodes of the global grid and improves the smoothness and quality of the approximation.

In this work the mean-squares piecewise polynomial approximation is based on the fifth degree BEM-polynomials. The MSPPA-6 algorithm is fulfilled in four stages.

1. An interval $[a,b]$ and the entire data set $\tilde{S}$ are divided into equal segments $[a,b]=\bigcup_{k=1}^{K}[x_{\alpha_k},x_{\beta_k}]$ and $\{\tilde{S}_i\}_{i=1}^{N}=\bigcup_{k=1}^{K}\{\tilde{S}_l^k\}_{l=1}^{N_k}$, where $N_k=\lfloor N/K\rfloor$, provided that $x_{\beta_{k-1}}\equiv x_{\alpha_k}$. The approximation function is found as the BEM-polynomial $P_{5\downarrow1}(x)=\mathbf{w}^T\mathbf{f}+\mathbf{b}^T\mathbf{r}$ at $\beta_k=-\alpha_k$. In this case basis functions do not change for $k=\overline{1,K}$. Vector $\mathbf{f}$ is fixed and $\mathbf{r}$ is free [7].

2. Calculation of $\hat{\mathbf{f}}_k=[\bar{f}_{\alpha_k},\bar{f}_{\beta_k},\bar{f}_{0_k}]^T$ by $2M+1$ nearest to the nodes of the grid $\Delta_3^{\alpha\beta}$ neighboring coordinates and data transformation $\tilde{S}_i^k\xrightarrow{\hat{\mathbf{f}}_k}\tilde{u}_i^k$, where k is the index of the segment:

$$\bar{f}_{\nu_k}=\frac{1}{2M+1}\sum_{l=-M}^{M}\tilde{S}_l^k,\quad \tilde{u}_i^k=\tilde{S}_i^k-\mathbf{b}_0^T\hat{\mathbf{f}}_k,$$
$$i=\overline{1,N_k},\quad f_\nu=f(\nu),\quad \nu=\alpha,\beta,0.$$

3. Calculation of $\hat{\mathbf{r}}_k$ applying the least-squares criterion

$$\sum_{i=N_{k-1}+1}^{N_k} [\tilde{u}_i^k - \mathbf{b}_k^T(\tau_i)\mathbf{r}_k]^2 \to \min_{\mathbf{r}_k}, \quad \tau_i \in [\alpha_k, \beta_k],$$

$$\hat{\mathbf{r}}_k = [\mathbf{B}^T\mathbf{B}]^{-1}\mathbf{B}^T\mathbf{u}^k, \quad \mathbf{b}_k \equiv \mathbf{b} = [b_1,\, b_2,\, b_3]^T,$$

where $\mathbf{u}^k = [u_1^k,\, u_2^k, \ldots, u_{N_k}^k]^T$ and $[\mathbf{B}^T\mathbf{B}]^{-1}$ is the normal matrix 3×3 for the kth segment:

$$[\mathbf{B}^T\mathbf{B}]^{-1} = \begin{bmatrix} \sum\limits_{j=1..N_k} b_{1j}^2 & \sum\limits_{j=1..N_k} b_{1j}\, b_{2j} & \sum\limits_{j=1..N_k} b_{1j}\, b_{3j} \\ \sum\limits_{j=1..N_k} b_{2j}\, b_{1j} & \sum\limits_{j=1..N_k} b_{2j}^2 & \sum\limits_{j=1..N_k} b_{2j}\, b_{3j} \\ \sum\limits_{j=1..N_k} b_{3j}\, b_{1j} & \sum\limits_{j=1..N_k} b_{3j}\, b_{2j} & \sum\limits_{j=1..N_k} b_{3j}^2 \end{bmatrix}.$$

4. Computation of the estimate $\hat{S}^k(x)$, according to the recovery formula

$$\hat{S}^k(x) = \mathbf{b}_0^T\, \hat{\mathbf{f}}_k + \mathbf{b}^T\, \hat{\mathbf{r}}_k, \quad k = \overline{1, K},$$

where

$$\mathbf{b}_0 = \left[-\frac{\tau(\tau-\beta)}{\alpha\gamma},\, \frac{\tau(\tau-\alpha)}{\gamma\beta},\, \frac{(\tau-\alpha)(\tau-\beta)}{\alpha\beta} \right]^T,$$

$$\mathbf{b} = \left[-\frac{\tau^2\,(\tau-\alpha)(\tau-\beta)^2}{\alpha\gamma},\, \frac{\tau^2\,(\tau-\alpha)^2(\tau-\beta)}{\gamma\beta},\, \frac{\tau\,(\tau-\alpha)^2(\tau-\beta)^2}{\alpha\beta} \right]^T.$$

Tests of the BEM approximation algorithm are presented in [5–8].

5. APPLICATIONS AND DISCUSSION

According to the MSPPA-6 algorithm presented there are two control parameters: K is the number of segments, and M is the number of samples $(2M+1)$ for the calculated components of vectors $\hat{\mathbf{f}}_k$. The results of variation of these parameters are shown in Figs. 5 and 6. In Fig. 5 the approximating curves of linear pulse energy increasing with some steps with different values of K and the same $2M+1$ are shown. In Fig. 6 the parameter K was fixed and $2M+1$ was varied.

For IBR-2M the full oscillation of pulse energy can be divided into two sets: slow changes and quick changes or noise. In Fig. 5 we can see that the parameter K is responsible for sensitivity of the method to changes.

Depending on the number of segments (K), the approximating curve can involve only a main trend (yellow line, Fig. 5) or include slow changes as well

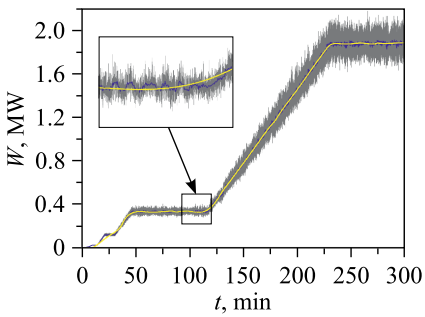

Fig. 5. Approximating curve as a function of the number of segments: gray — pulse power, yellow — $K = 13$, $2M+1 = 201$, blue — $K = 1344$, $2M + 1 = 201$ for regular increase of power of the IBR-2M

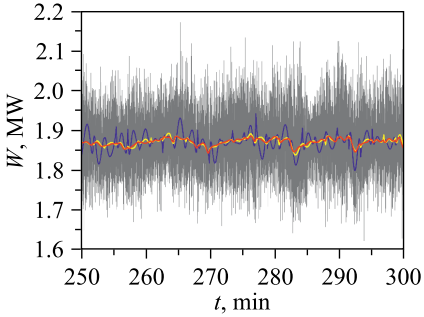

Fig. 6. Approximating curve as a function of $2M + 1$, $K = 335$: gray — pulse power, blue — $2M+1 = 9$, red — $2M+1 = 51$, yellow — $2M + 1 = 201$

(blue line, Fig. 5). The second set of parameters M, α and β (see section 3) is responsible for sensitivity of the method to the level of noise. It should be mentioned, beginning with $2M + 1 = 51$, there is no big difference between approximating curves with the same K — the maximal deviation is 1.5% (Fig. 6).

As was said above, increasing the number of segments allows revealing changes of the pulse energy induced by a slowly varying source, but if the number of segments is too high, the noise is let through the baseline. Revealing the most suitable K is a critical issue.

It was mentioned earlier that the baseline has to contain impacts of control rods on the oscillation of the reactor power. For IBR-2M the main source of slow changes of the pulse energy is the automatic regulator (AR), which is used for automatic level control. Therefore, an assessment criterion for choosing the parameter K is the presence of pulse energy changes induced by shifts of the AR position. Since the baseline only involves low frequencies we can estimate the optimal parameter K by varying the contribution of the low-frequency component of the reactor noise (0–2.5 Hz) to the total noise:

$$\frac{D_{0-0.25}}{D} = \frac{\int\limits_0^{0.25} S(f)\,df}{\int\limits_0^{2.5} S(f)\,df},$$

where S is the spectral density of the reactor noise and D its integral over specific ranges. Figure 8 shows this ratio (curve *1*) together with its derivative $d(D_{0-0.25}/D)/dK$ for the same 240–320 min time period also shown in Figs. 5 and 7. For small K there is a gradual decrease in very low frequencies, as the

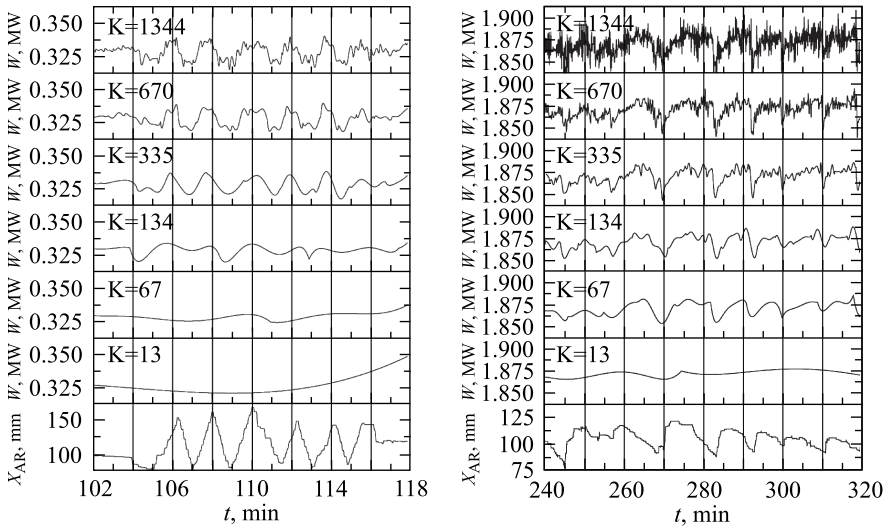

Fig. 7. Different approximating curves and positions of the automatic regulator (bottom), $2M + 1 = 201$

baseline is taken out. After a while, in the $K = 700{-}900$ region, the impact of K diminishes and we interpret this as an exhaustion of the potential K on the data. The optimal K can be found in this region by

$$d(D_{0-0.25}/D)/dK = 0.$$

K, the number of segments, effectively models a polynomial order, hence its further increase is equivalent to fitting a higher order polynomial. Higher order polynomials can be Taylor-series like, or Fourier-series like. Effectively, reaching higher orders means including Fourier components (of the noise) without declaring them. However, the acception of baseline is more Taylor-series in nature (quadratic, cubic, etc.). Therefore, we attribute the further decrease of the ratio seen in Fig. 8 to baseline over-modeling (to include Fourier components) and claim that $d(D_{0-0.25}/D)/dK = 0$ serves an optimal value for K.

The maximum of $(D_{0-0.25}/D)'$ corresponds to the optimal value of the parameter K ($K = 802$). But the area of the maximum is quite flat; therefore, we can say that the optimum of the parameter K ranges from 700 to 900 segments. A lower number of segments leaves the baseline component in the noise spectrum, while an increase in the number of segments above the optimal value involves cutting low noise frequencies together with frequencies of the baseline. The analysis of other intervals of the signal (data) resulted in the same value.

The result of baseline extraction is presented in Figs. 9 and 10: the spectral density of initial data (signal) and of the reactor noise (Fig. 9), and the spectral

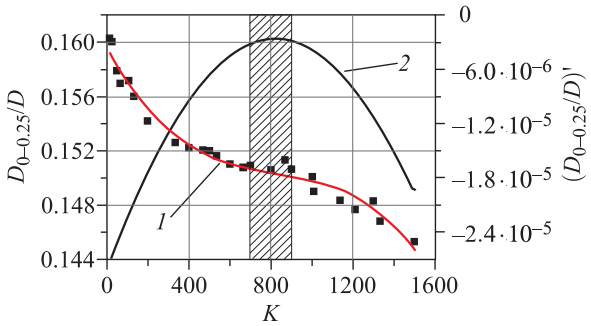

Fig. 8. Dependence of the contribution of the low-frequency component of reactor noise, $D_{0-0.25}/D$ (*1*), and of the rate of its change, $d(D_{0-0.25}/D)/dK$ (*2*), on the parameter K. The highlighted area indicates the optimal values of the parameter K

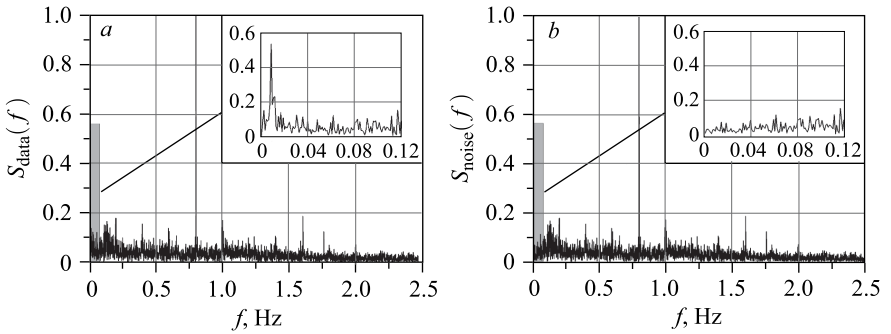

Fig. 9. Spectral density of initial data (signal) (*a*) and of reactor noise (*b*)

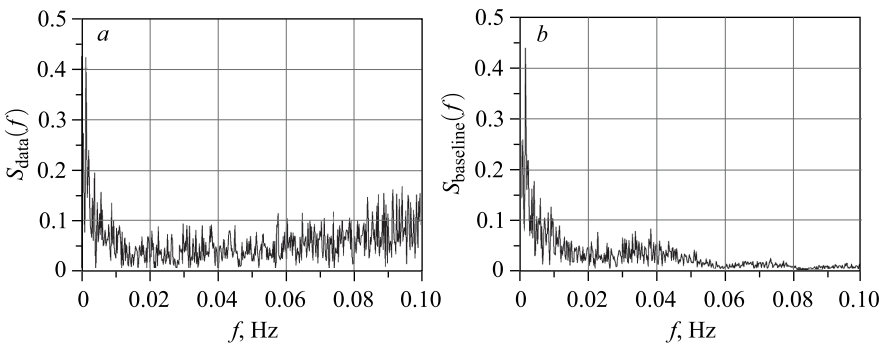

Fig. 10. Spectral density of initial data (signal) (*a*) and of the baseline $K = 802$, $2M+1 = 201$ (*b*) in the range of 0–0.1 Hz

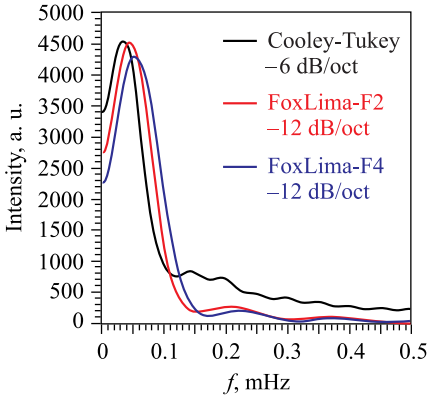

Fig. 11. Spectral density of the baseline ($K = 802$, $2M + 1 = 201$) in the range of 0–0.5 mHz

density of initial data (signal) and the baseline $K = 802$, $2M + 1 = 201$ in the range of 0–0.1 Hz (Fig. 10).

The peak very close to zero is zoomed on in Fig. 11 — processed with an in-house oversampling FFT method using Fourier-space apodization (algorithms F2 and F4 in Fig. 11). It can be seen how these algorithms reduce the Cooley-Tukey tails (and ripples from the Gibbs satellites), giving good estimates in the integrals of the spectrum.

6. CONCLUSIONS

The MSPPA-6 algorithm for neutron noise baseline detection, based on the Basic Element Method, has been presented. The algorithm was applied to both static and dynamic states of the reactor within a power range of 30 kW to 2 MW. The algorithm depends on two control parameters, K and $2M + 1$. Their optimal values were determined so that the baseline (mostly due to control-rods activity) does not pass into the noise spectrum, nor it contains the lower frequency components of the noise spectrum. The MSPPA algorithm is a flash-algorithm due to its analyticity. The average run-time is approximately 0.05 ms/point on x86_64 Intel Core i5-4570 Sandy Bridge machine at 3.20 GHz.

BEM-polynomials applied to a batch of data from the IBR-2M reactor revealed their usefulness in the analysis of slow trends. This is very important, as degradation in systems is a slow-trend process.

REFERENCES

1. *Bernitt P.* In-Core Neutron Noise Analysis for Diagnosis of Fuel Assembly Vibrations. Thesis for the Degree of Master of Science. Chalmers University of Technology, Sweden, 2008. CTH-NT-218.

2. *Pepelyshev Y. N., Taiybov L. A., Garibov A. A. et al.* // At. Energy. 2013. V. 113. P. 248; https://doi.org/10.1007/s10512-013-9625-y.
3. *Pepelyshev Yu. N., Tsogtsaikhan Ts.* The Noise Effects of Liquid Sodium Coolant System of IBR-2M on Reactivity Fluctuation. JINR Commun. P13-2014-61. Dubna, 2014 (in Russian).
4. *Pepelyshev Yu. N., Tsogtsaikhan Ts.* Investigation of the Dynamics of Pulse Energy Noise at the IBR-2M Reactor in the Fuel Burnup. JINR Commun. P13-2017-4. Dubna, 2017 (in Russian).
5. *Dikusar N. D.* The Basic Element Method // Math. Models Comput. Simulations. 2011. V. 3, No. 4. P. 492–507; http://link.springer.com/article/10.1134.%2FS2070048211040053.
6. *Dikusar N. D.* Optimization of the Solution in Problems of Piecewise Polynomial Approximation // Supercomputing and Mathematical Modeling: Proc. of the XVI Intern. Conf. / Ed. R. M. Shagaliyev. Sarov: FSUE "RFNC-VNIIEF", 2017. P. 113–122; http://wwwinfo.jinr.ru/publish/Preprints/2016/085(P11-2016-85).pdf, (in Russian).
7. *Dikusar N. D.* Piecewise Polynomial Approximation of the Sixth Order with Automatic Knots Detection // Math. Models Comput. Simulations. 2014. V. 6, No. 5. P. 509–522; http://link.springer.com/article/10.1134.%2FS2070048214050020.
8. *Dikusar N. D.* Higher-Order Polynomial Approximation // Math. Models Comput. Simulations. 2016. V. 8, No. 2. P. 183–200; http://link.springer.com/article/10.1134/S2070048216020058.

Received on April 11, 2018.

Редактор *Е. И. Кравченко*

Подписано в печать 02.07.2018.
Формат 60 × 90/16. Бумага офсетная. Печать офсетная.
Усл. печ. л. 0,93. Уч.-изд. л. 1,05. Тираж 215 экз. Заказ № 59433.

Издательский отдел Объединенного института ядерных исследований
141980, г. Дубна, Московская обл., ул. Жолио-Кюри, 6.
E-mail: publish@jinr.ru
www.jinr.ru/publish/